HAL
open science

Design and experimental evaluation of a dynamically balanced redundant planar 4-RRR parallel manipulator

Volkert van Der Wijk, Sébastien Krut, François Pierrot, Just Herder

To cite this version:

Volkert van Der Wijk, Sébastien Krut, François Pierrot, Just Herder. Design and experimental evaluation of a dynamically balanced redundant planar 4-RRR parallel manipulator. The International Journal of Robotics Research, 2013, pp.743-758. 10.1177/0278364913484183 . lirmm-00822698

HAL Id: lirmm-00822698

https://hal-lirmm.ccsd.cnrs.fr/lirmm-00822698

Submitted on 4 Jun 2013

HAL is a multi-disciplinary open access archive for the deposit and dissemination of scientific research documents, whether they are published or not. The documents may come from teaching and research institutions in France or abroad, or from public or private research centers.

L'archive ouverte pluridisciplinaire **HAL**, est destinée au dépôt et à la diffusion de documents scientifiques de niveau recherche, publiés ou non, émanant des établissements d'enseignement et de recherche français ou étrangers, des laboratoires publics ou privés.

Design and experimental evaluation of a dynamically balanced redundant planar 4-RRR parallel manipulator

Journal:	*International Journal of Robotics Research*
Manuscript ID:	IJR-12-1488.R1
Manuscript Type:	Original Article
Date Submitted by the Author:	11-Dec-2012
Complete List of Authors:	Wijk, Volkert; University of Twente, Laboratory of Mechanical Automation, Design of Mechanisms and Robotics Krut, Sébastien; LIRMM, Robotics Department Pierrot, François; LIRMM, Robotics Department Herder, Just L.; University of Twente, Mechanical Automation, Design of Mechanisms and Robotics
Keyword:	Parallel Robots < Mechanics, Design and Control, Dynamics < Mechanics, Design and Control, Mechanism Design < Mechanics, Design and Control
Abstract:	Shaking forces and shaking moments in high speed parallel manipulators are a significant cause of base vibrations. These vibrations can be eliminated by designing the manipulator to be shaking-force balanced and shaking-moment balanced. In this article an approach for the design and for the evaluation of high speed dynamically balanced parallel manipulators is presented and applied for a comparative experimental investigation of the balanced and the unbalanced DUAL-V planar 4-RRR parallel manipulator. For precise simulation of the manipulator motion, the inverse dynamic model of the manipulator is derived and validated. Experiments show that the balanced manipulator has up to 97% lower shaking forces and up to a 96% lower shaking moment. For small inaccuracies of the counter-masses or for a small unbalanced payload on the platform, base vibrations may be considerable for high speed manipulation, however their values remain significantly low as compared to the unbalanced manipulator. For the balanced manipulator the actuator torques are about 1.6 times higher and the bearing forces are about 71% lower as compared to the unbalanced manipulator.

Note: The following files were submitted by the author for peer review, but cannot be converted to PDF. You must view these files (e.g. movies) online.
DUAL-V.avi

SCHOLARONE™
Manuscripts

For Peer Review

Design and experimental evaluation of a dynamically balanced redundant planar 4-RRR parallel manipulator

Volkert van der Wijk§, Sébastien Krut‡, François Pierrot‡, Just L. Herder§
§ Lab. of Mechanical Automation and Mechatronics, University of Twente, The Netherlands
‡ LIRMM, Montpellier, France
v.vanderwijk@utwente.nl, sebastien.krut@lirmm.fr,
francois.pierrot@lirmm.fr, j.l.herder@utwente.nl

For Peer Review

Abstract

Shaking forces and shaking moments in high speed parallel manipulators are a significant cause of base vibrations. These vibrations can be eliminated by designing the manipulator to be shaking-force balanced and shaking-moment balanced. In this article an approach for the design and for the evaluation of high speed dynamically balanced parallel manipulators is presented and applied for a comparative experimental investigation of the balanced and the unbalanced *DUAL-V* planar 4-RRR parallel manipulator. For precise simulation of the manipulator motion, the inverse dynamic model of the manipulator is derived and validated.

Experiments show that the balanced manipulator has up to 97% lower shaking forces and up to a 96% lower shaking moment. **For small inaccuracies of the counter-masses or for a small unbalanced payload on the platform, base vibrations may be considerable for high speed manipulation, however their values remain significantly low as compared to the unbalanced manipulator.** For the balanced manipulator the actuator torques are about 1.6 times higher and the bearing forces are about 71% lower as compared to the unbalanced manipulator.

Key words: shaking force balancing, shaking moment balancing, parallel manipulator, actuator torques, bearing forces, experiments

1. Introduction

During the last decades parallel manipulators (i.e. robots) have found their way into industry for applications such as fast pick and place tasks. The continuous demand for increased operational speeds of these robots challenges the

designer with various issues. One of them is the severe vibration in the base due to the shaking forces and the shaking moments, i.e. the inertial forces and moments exerted by the manipulator to the base, in practice, major cause of wear and failure of the manipulator, its control system, and neighboring machines. Common solutions to reduce the influence of these vibrations are by increasing the stiffness and mass of the base, by applying damping, and by sophisticated control. Another solution, that eliminates the source of vibrations at its roots, is to design the parallel manipulator such that, for all motion, the shaking forces and the shaking moments are minimal or zero. Such a manipulator is said to be dynamically balanced and is characterized in having both the sum of linear momentum and the sum of angular momentum of all elements be constant for all motion (Van der Wijk et al. (2009)).

Contrary to the dynamic balancing of mechanisms, a topic being investigated for well over a century (Arakelian and Smith (2005a), Arakelian and Smith (2005b)), the dynamic balancing of manipulators and in particular the dynamic balancing of parallel manipulators started rather **recently**. The shaking-force balancing of the serial manipulator PUMA-760 was studied at the end of the 1980's in (Chung and Cho (1988), Lim et al. (1989), Lim et al. (1990)). In 1996 the shaking-force balancing of a three-degree-of-freedom (3-DoF) planar parallel manipulator was investigated in (Jean and Gosselin (1996)). In 2000 the dynamic balancing of parallel manipulators was first treated in a more general way in (Ricard and Gosselin (2000)). Although various articles have been published afterwards, the total volume of related literature is considerably small. In addition, most of the literature investigates the balancing of multi-DoF manipulators by application of balance solutions for mechanisms, which has shown to have considerable disadvantages regarding additional mass, inertia, and complexity (Van der Wijk et al. (2009)). Recently balance solutions that take advantage of the parallel structure of manipulators were shown to have significant potential (Van der Wijk and Herder (2012b), Van der Wijk et al. (2011), Van der Wijk and Herder (2012a)).

Also most literature on dynamic balancing, both for mechanisms and for manipulators, are theoretical, there are relatively few experimental results. Regarding serial manipulators, in (Chung and Cho (1988)) the experiments on the PUMA-760 showed that shaking-force balance reduced the actuator torques significantly since actuators do not have to compensate gravity forces. The inertia increased with balancing, but it was found that the actuator torques due to coulomb friction were dominating, for which the inertia increase was found acceptable. Because of lower actuator torques, in (Lim et al. (1989)) it was experimentally shown that shaking-force balance is advantageous for the accuracy of the dynamic identifica-

For Peer Review

tion of the unbalanced robot. The balanced PUMA-760 also showed to have a nine times higher payload capacity, or the ability of moving at double accelerations and at about three times higher velocities (Lim et al. (1990)).

Regarding parallel manipulators, in Agrawal et al. (2001) a shaking-force balanced parallel mechanism based on the principal vector linkage of Fischer (Fischer (1906)) was presented and tested. Although presented as a balanced serial chain, it can be regarded as a force-balanced parallel manipulator. The center-of-mass (CoM) of the linkage is an invariant point in one of the joints, which was verified by moving the mechanism in a statically balanced way while measuring the joint angles.

In (Foucault and Gosselin (2004)) a dynamically balanced 3-DoF planar parallel manipulator was presented and tested. The manipulator is composed of two independently force-balanced parallelograms pivoted to the base and coupled with an end-effector link. Shaking-moment balance was achieved with separate counter-rotating inertias (inertia-wheels). The manipulator was suspended by vertical cables for which it could float within the horizontal plane and it was actuated at a low speed corresponding to the eigenmotion of this suspension. The motion of a point in the base of the manipulator was measured to verify the balance performance.

The goal of this article is to present an approach for the design and for the evaluation of high-speed dynamically-balanced parallel manipulators, and to apply this approach for a comparative experimental investigation of the balanced and the unbalanced *DUAL-V* planar 4-RRR parallel manipulator.

In addition to the balance performance, other important aspects such as the influence of the balance elements on the actuator torques and on the bearing forces are investigated. Also the sensitivity of the balance parameters and the influence of payload are evaluated.

First the design and evaluation approaches are presented followed by the detailed design of the balanced DUAL-V manipulator. For this manipulator the exact inverse dynamic model is derived and validated and used for precise simulations without the need of a controller. The experimental setup and the experiments are described and the experimental results are presented and discussed.

2. Approach to the design and evaluation of a balanced manipulator

This section presents and discusses the approaches to the design and the evaluation of high-speed balanced parallel manipulators which are applied for investigation of the planar 4-RRR parallel manipulator.

For Peer Review

2.1. Design

To take advantage of the parallel architecture for the purpose of dynamic balance, the common way of balancing - to first consider solely the kinematics of the manipulator and subsequently its balancing - is not effective and efficient. When, after all efforts to balance a given architecture, the balance solutions are not applicable, the kinematics will have to be considered all over again. Considering balance properties in the very beginning of the kinematic design therefore is essential. In (Demeulenaere and Berkof (2008)) suggestions into this direction have been proposed for the field of input-torque balancing of machines. Moreover, for multi-DoF manipulators the kinematics often is not as determining as it is for single-DoF mechanisms. Although for example the useful workspace of a manipulator depends on the kinematic design, often a wide variety of kinematic designs are applicable to carry out the intended tasks. Especially with the target for high speed manipulators, this should be used in our advantage.

Since for dynamic balance the sum of the linear momentum and the sum of the angular momentum of all manipulator elements need to be constant, dynamic balance is all about similar opposite motion of masses and inertias. This means that from a kinematic point of view elements need to counter-rotate and to counter-move with respect to one-another. The more the motions are similar and opposite, the better the balanced solution can be. The level of similar opposite motion depends on the mass distribution in each element. Additional balance elements such as counter-masses and counter-inertias can be advantageous for tuning the mass distributions. However for low mass, low inertia, and low complexity they should only be applied to elements connecting the base (Van der Wijk and Herder (2009)).

The design of a balanced manipulator can be approached in two ways. If an initial kinematic architecture of the manipulator is known, the kinematic parameters can be adapted by rearranging the locations of the base pivots and by changing the dimensions of the elements to induce and to improve counter-motion of elements. Accordingly the mass distributions can be adapted to induce and improve balance. This means that both the kinematic parameters and the mass parameters in the equations of the linear momentum and the angular momentum are adapted. With this approach it is also possible to obtain best compromises between kinematics and balance, especially when perfect balance is not required.

A second approach is to derive balanced manipulators from known balanced architectures such as (pantograph-based) principal vector linkages (Van der Wijk and Herder (2012b)) or other inherently balanced linkages (Van der Wijk and

For Peer Review

Herder (2012a)). These architectures are based on the essential kinematic relations for balance and as long as these relations are maintained, any manipulator that is derived is balanced. This approach is specifically interesting for synthesis of a wide variety of kinematic solutions with perfect balance capability. Both approaches will be employed for the balancing of the planar 4-RRR parallel manipulator.

2.2. *Evaluation and comparative study*

To verify if theoretical results are correct, the first step of the evaluation of the balanced manipulator is to measure the balance performance. The shaking forces and shaking moments can be obtained from a multi-body simulation with an accurate model of the prototype manipulator or from measurements in an experimental setup. From the fabrication process of the prototype manipulator and from the obtained balance precision the costs of the balance solution in terms of structural design and production effort can be derived together with the sensitivity to balance inaccuracies. For the potential of the manipulator it is important to also investigate and measure the required driving power (actuator torques) and the bearing forces, which determine the structural demand on the design, e.g. the size of the actuators and the stiffness of the system.

For both the evaluation and the comparative investigation, it is important to exclude the influence of the controller and the control design. Although a controller is required to move the manipulator and in practice it will never move the manipulator exactly as desired, the shaking forces and shaking moments do not depend on the controller directly. They depend solely on the actual motion of the manipulator. This means that even with a bad controller the balance performance can be evaluated well when the real motion of the manipulator is considered and measured and also is used as input in the simulations.

To validate the measured results, the measured manipulator motion can be simulated precisely with a multi-body dynamic model when the exact inverse dynamics are known. Then the design of a controller for the simulation is omitted since open-loop control can be applied, calculating the required actuator torques at each time step.

Also the bearing forces do not depend on the controller directly but they depend on the real motion of the manipulator. In practice it is challenging to measure the bearing forces in an experimental setup but they can be estimated from a precise simulation of the measured manipulator motion.

For Peer Review

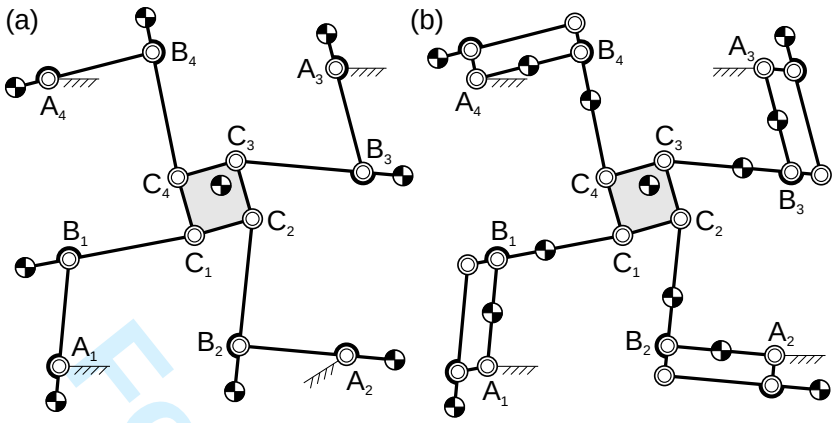

Figure 1: Planar 4-RRR manipulator with common force-balance principles to have the CoM of each of the four arms with part of the platform mass in fixed pivots A_i with (a) counter-masses in each link of the arms and with (b) pantograph arms with a counter-mass.

3. Design of the DUAL-V manipulator

In this section the two design approaches are applied for the synthesis of a balanced redundant 3-DoF planar 4-RRR parallel manipulator. Figure 1a shows the typical design of a 3-DoF planar 4-RRR parallel manipulator which consists of four 2-DoF arms (or dyads) i connecting the moving platform (or end-effector) $C_1C_2C_3C_4$ with four pivots A_i to the fixed base. With an actuator in each of the four fixed pivots, the manipulator has one degree of actuation redundancy. This is advantageous since manipulators with actuation redundancy have an increased acceleration capability and have more homogeneous dynamic characteristics (e.g. force transmission to the platform) throughout the workspace (Corbel et al. (2010)).

Figures 1a and 1b show how this manipulator is force-balanced when common balance principles for mechanisms are applied. For the balance solution in Fig. 1a **the CoM of each link B_iC_i is located such that the CoM of this link together with part of the platform mass modeled in C_i is in B_i, and the CoM of each link A_iB_i is located such that the CoM of this link together with both the mass of link B_iC_i and part of the platform mass modeled in B_i is in A_i, which can be achieved with additional counter-masses in each of the links** (Van der Wijk et al. (2011)). In Fig. 1b each of the four arms is balanced with a single counter-mass and additional parallel links **which therefore result in pantograph linkages**

For Peer Review

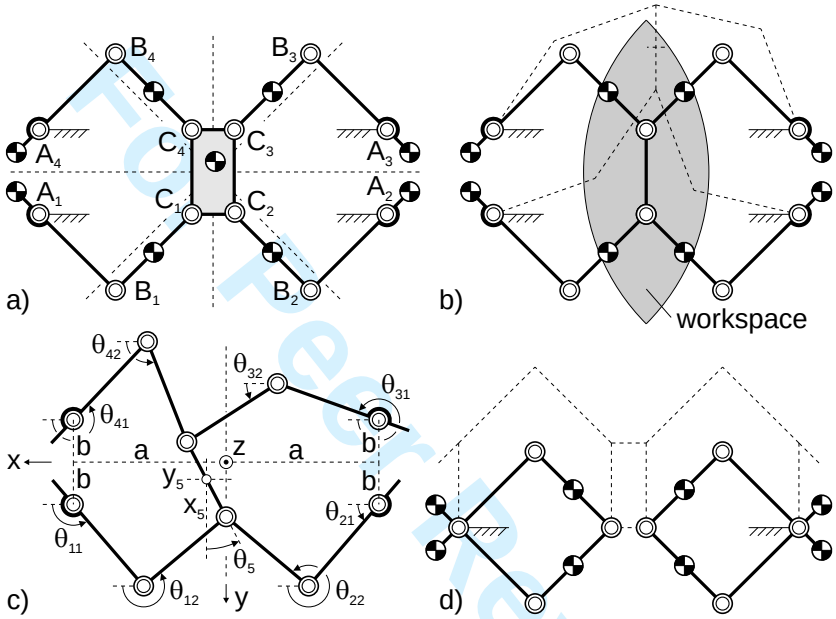

Figure 2: a) Specific kinematic solution such that for translational motion of a non-rotated platform force-balance is obtained with solely counter-masses in elements connecting the base; b) Compact DUAL-V configuration **where platform joints coincide**; c) Definition of the kinematic variables and the parameters of the base; d) Synthesis of the DUAL-V configuration from two force-balanced pantographs.

For Peer Review

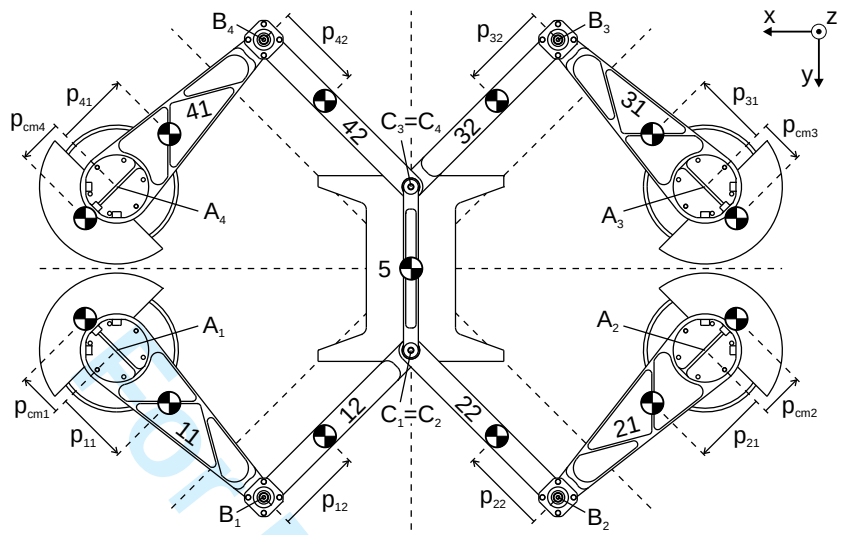

Figure 3: CAD of DUAL-V prototype manipulator with parameter definitions (patent pending).

of which the CoM of the links, counter-mass, and part of the platform mass is in A_i (Van der Wijk and Herder (2008), Briot et al. (2009)). This solution showed to be advantageous for low mass and low inertia at the cost of an increased complexity (Van der Wijk et al. (2009)).

Instead of adding a parallelogram to each of the four arms as in Fig. 1b, the arms can also be designed and arranged such that two pairs of arms each form a parallelogram as shown in Fig. 2a. When the manipulator moves, the parallelograms are maintained for all translations throughout the workspace when the platform is not rotated. This solution can be derived from the linear momentum equations of the manipulator (Van der Wijk et al. (2011)), **which for force-balance are constant. Since the motion of parallel links is linearly related, the linear momentum equations are reduced and result in a force-balance solution where each pair of arms is balanced with two counter-masses in the links connecting the base.** Then the 4-RRR manipulator can be force-balanced with four counter-masses in total.

For a platform rotation ($\theta_5 \neq 0$) the parallelograms are not maintained. This means that motion with a rotated platform is not perfectly force-balanced. Since for rotations of the platform the pairs of arms remain close to a parallelogram, the force balance still can be expected to be advantageous.

For Peer Review

Because of the symmetric kinematic design, **when the 4-RRR manipulator moves along the orthogonal axes without rotation, all links connecting the base counter-rotate linearly with one another and also all links connecting the platform counter-rotate linearly with one another. This means that when the links in each of these two groups have equal inertia, they balance out their shaking moments and the manipulator then is also perfectly shaking-moment balanced for these motions. For motion with non-rotated platform along the diagonal axes, the links counter-rotate almost linearly with one another for which the manipulator is almost perfectly shaking-moment balanced for these motions. To have four arms instead of the minimum of three arms for a 3-DoF manipulator therefore is not only beneficial for actuation redundancy, but also to obtain a symmetric kinematic and dynamic design that is beneficial for dynamic balance.** Motion with rotated platform or off the orthogonal axes is not perfectly moment-balanced. **Since the motion remains in the vicinity** of perfect dynamic balance, also here the balance performance can be expected to be advantageous.

For improved force transmission to the platform and for compactness of the manipulator, the platform **can be reduced to a link with coinciding joints** as shown in Fig. 2b. This configuration is named the 'DUAL-V' manipulator.

The synthesis so far was based on the first design approach of adapting the kinematic parameters and the mass parameters of an initial kinematic architecture. Synthesis based on the second approach is illustrated in Fig. 2d. Here the DUAL-V configuration is composed of two force-balanced pantographs, i.e. composed of known balanced architectures which can be adapted to the DUAL-V design without affecting the balance capabilities of the pantographs. This is since pantographs keep their balance properties for any adaption as long as the parallelograms are maintained for all motion.

A prototype of the DUAL-V manipulator was designed and fabricated with the parameters in Table 1. **These parameters and the kinematic variables of the manipulator are illustrated in Fig. 2c and Fig. 3, of which the latter** shows the top-view of the CAD of the prototype manipulator. **All arm links** $i1$ **and** $i2$ **have equal lengths** l_{i1} **and** l_{i2}**, respectively, the fixed pivots are located at distances** $a = l_{i1}\sqrt{2}$ **and** b **with respect to the center, and the platform link** 5 **has a length** $l_5 = 2b$**.** With these parameters the pairs of arms are parallelograms for motion along the orthogonal axes with non-rotated platform. The theoretical workspace of the manipulator for the given dimensions is shown in Fig. 2b and consists of the intersection of two circles with radii $l_{i1} + l_{i2} = 0.56m$ of which the maximal width along x is $2(l_{i1} + l_{i2} - a) = 0.328m$ and the maximal width

For Peer Review

along y is $2\sqrt{(l_{i1}+l_{i2})^2-a^2} = 2a = 0.792m$. Due to collisions, the motion of the prototype along x is limited to a workspace width of $0.288m$.

The links of the manipulator are made of aluminium and were designed and produced before the counter-masses. Together with all bolts, nuts, bearings, etc., they were measured with a 0.01mm accurate digital caliper and weighted with a 0.01g accurate balance. Together with the CAD model in SolidWorks the parameters of the link CoMs p_{i1} and p_{i2}, the masses of the links m_{i1}, m_{i2}, and m_5, and their inertia about their CoM I_{i1}, I_{i2}, and I_5 were determined.

Subsequently the counter-masses were designed of circular segments made of brass. Their required mass $m_{cm,i}$ and CoM location at distance $p_{cm,i}$ relative to A_i were calculated with the force-balance conditions which for the first design approach are derived from (Van der Wijk et al. (2011)) as

$$\begin{aligned}
m_{11}p_{11} + m_{12}l_{11}(1-\tfrac{p_{12}}{l_{12}}) + m_{42}p_{42} + m_{32}l_{42}\tfrac{p_{32}}{l_{32}} + m_5\tfrac{l_{42}}{2} &= m_{cm,1}p_{cm,1}\\
m_{21}p_{21} + m_{22}l_{21} + m_{12}l_{21}\tfrac{p_{12}}{l_{12}} + \tfrac{m_5}{2}l_{21} &= m_{cm,2}p_{cm,2}\\
m_{31}p_{31} + m_{32}l_{31}(1-\tfrac{p_{32}}{l_{32}}) + m_{22}p_{22} + m_{12}l_{22}\tfrac{p_{12}}{l_{12}} + m_5\tfrac{l_{22}}{2} &= m_{cm,3}p_{cm,3}\\
m_{41}p_{41} + m_{42}l_{41} + m_{32}l_{41}\tfrac{p_{32}}{l_{32}} + \tfrac{m_5}{2}l_{41} &= m_{cm,4}p_{cm,4}
\end{aligned} \tag{1}$$

and from the second design approach are derived from (Van der Wijk and Herder (2012b)) as

$$\begin{aligned}
m_{11}p_{11} + m_{12}l_{11} + m_{42}p_{42} + m_5\tfrac{l_{11}}{2} &= m_{cm,1}p_{cm,1}\\
m_{21}p_{21} + m_{22}l_{21} + m_{32}p_{32} + m_5\tfrac{l_{21}}{2} &= m_{cm,2}p_{cm,2}\\
m_{31}p_{31} + m_{32}l_{31} + m_{22}p_{22} + m_5\tfrac{l_{31}}{2} &= m_{cm,3}p_{cm,3}\\
m_{41}p_{41} + m_{42}l_{41} + m_{12}p_{12} + m_5\tfrac{l_{41}}{2} &= m_{cm,4}p_{cm,4}
\end{aligned} \tag{2}$$

which both give equal results.

The main aim of the design of the counter-masses was to have the reduced inertia $I_{cm,i} + m_{cm,i}p_{cm,i}^2$ of each counter-mass relative to A_i be as low as possible since this is advantageous for low actuator torques (Van der Wijk et al. (2012)). Therefore a high mass of each counter-mass with its CoM as close to A_i as possible is needed. A counter-mass material with high density such as brass and a design which can be large in the out-of-plane direction (thick counter-masses) then are advantageous. The design of the counter-masses was verified with the mass properties function in SolidWorks, with which it was also verified that the common CoM of the complete manipulator is at the same location for any position in the workspace with non-rotated platform.

For Peer Review

Each counter-mass was designed such that part of its mass $m_{tun,i} = 0.188kg$ is a separate element made of lead, placed at a distance $p_{tun,i} = 0.080m$ from A_i on top of the brass segments. This was done to fine-tune the counter-masses compensating for production inaccuracies and to be able to remove a small mass for experiments of the balance performance with non-perfect counter-masses. The mass and inertia of these tuning masses are included in the parameters $m_{cm,i}$ and $I_{cm,i}$ in Table 1.

Table 1: DUAL-V parameters

[m]	[kg]	[kgm^2]	[m]
$l_{i1} = 0.2800$	$m_{i1} = 1.169$	$I_{i1} = 0.012967$	$p_{i1} = 0.0737$
$l_{i2} = 0.2800$	$m_{i2} = 0.606$	$I_{i2} = 0.006417$	$p_{i2} = 0.1279$
$l_5 = 0.2200$	$m_5 = 0.899$	$I_5 = 0.008168$	$p_{cm,i} = 0.0575$
$a = 0.3960$	$m_{cm,i} = 7.983$	$I_{cm,i} = 0.026845$	$p_{tun,i} = 0.080$
$b = 0.1100$	$m_{tun,i} = 0.188$	$I_{act,i} = 0.004100$	

4. Inverse dynamic model and validation with simulation model

In this section the inverse dynamic model of the DUAL-V is derived and validated with a multi-body simulation.

4.1. Inverse dynamic model to derive the actuator torques

The motion of the platform of the DUAL-V can be prescribed with $\overline{u} = [x_5(t), y_5(t), \theta_5(t)]^T$ with the position of the center of the platform (x_5, y_5) and the orientation of the platform θ_5 relative to the xy-reference frame at a time t, as illustrated in Fig. 2c. The actuator torques $\overline{\tau}$ required at a time t for a prescribed motion $\overline{u}$ can be calculated as a combination of three individual parts as

$$\overline{\tau} = \overline{\tau}_I + \overline{\tau}_{II} + \overline{\tau}_{III} \tag{3}$$

Here $\overline{\tau}_I$ is the required actuator torque to move the platform and part of the mass of links $i2$, $\overline{\tau}_{II}$ is the required actuator torque to move links $i1$ and part of the mass of links $i2$, and $\overline{\tau}_{III}$ is the required actuator torque of part of the rotational motion of links $i2$. This approach follows from (Corbel et al. (2010)) and is extended to being exact by not simplifying the dynamics of the links $i2$. Similar to (Corbel

For Peer Review

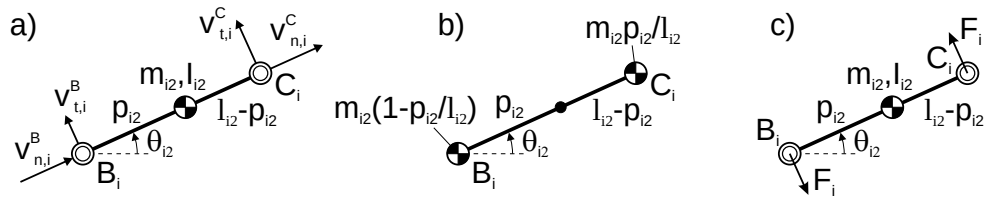

Figure 4: a) Velocity vectors of joints B_i and C_i of links $i2$; b) Equivalent mass model of links $i2$; c) Forces F_i in joints B_i and C_i for rotational acceleration of links $i2$.

et al. (2010)), the mass of links $i2$ is distributed equivalently to joints B_i and C_i and is included in both $\overline{\tau}_I$ and $\overline{\tau}_{II}$. However the rotational inertia of links $i2$ then is not completely considered. $\overline{\tau}_{III}$ therefore is the torque required to include the rotational inertia of links $i2$ exactly, as will become clear later on.

4.1.1. Actuator torques $\overline{\tau}_I$ for the motion of the platform

The actuator torques $\overline{\tau}_I$ for the motion of the platform can be calculated from the equations of the power of the actuator torques $\overline{\tau}_I$ that has to be equal to the power of the motion of the platform, which is written as

$$\dot{\overline{q}}^T \overline{\tau}_I \;=\; \dot{\overline{u}}^T \overline{F}_p \tag{4}$$

where $\dot{\overline{q}} = [\dot{\theta}_{11}, \dot{\theta}_{21}, \dot{\theta}_{31}, \dot{\theta}_{41}]^T$ is the vector of the angular velocities of the driven links $i1$, $\dot{\overline{u}} = [\dot{x}_5, \dot{y}_5, \dot{\theta}_5]^T$ is the vector of the velocities of the platform motion, and $\overline{F}_p$ is the vector of the resultant forces and the resultant moment that act on the platform. For a prescribed motion of the platform, $\dot{\overline{q}}$ can be derived from the velocity vectors of joints B_i and C_i along the line B_iC_i which, for a rigid link, are equal. These vectors are shown in Fig. 4a and are written and calculated as

$$v^B_{n,i} = v^C_{n,i} \qquad \rightarrow \qquad \overline{X}_n \dot{\overline{q}} \;=\; \overline{Y}_n \dot{\overline{u}} \tag{5}$$

with

$$\overline{X}_n = \begin{bmatrix} -l_{11}s(\theta_{11}-\theta_{12}) & 0 & 0 & 0 \\ 0 & -l_{21}s(\theta_{21}-\theta_{22}) & 0 & 0 \\ 0 & 0 & -l_{31}s(\theta_{31}-\theta_{32}) & 0 \\ 0 & 0 & 0 & -l_{41}s(\theta_{41}-\theta_{42}) \end{bmatrix} \tag{6}$$

For Peer Review

$$\overline{Y}_n = \begin{bmatrix} c(\theta_{12}) & s(\theta_{12}) & -c(\theta_{12}-\theta_5)b \\ c(\theta_{22}) & s(\theta_{22}) & -c(\theta_{22}-\theta_5)b \\ c(\theta_{32}) & s(\theta_{32}) & c(\theta_{32}-\theta_5)b \\ c(\theta_{42}) & s(\theta_{42}) & c(\theta_{42}-\theta_5)b \end{bmatrix} \tag{7}$$

Here $s()$ and $c()$ are used as shorthand notation for $\sin()$ and $\cos()$, respectively, and b is the parameter in Table 1. From Eq. (5) $\dot{\overline{q}}$ then is derived as

$$\dot{\overline{q}} = \overline{X}_n^{-1}\overline{Y}_n\dot{\overline{u}} = \overline{J}\dot{\overline{u}} \tag{8}$$

in which $\overline{J}$ is the jacobian matrix

$$\overline{J} = \begin{bmatrix} \frac{-c(\theta_{12})}{l_{11}s(\theta_{11}-\theta_{12})} & \frac{-s(\theta_{12})}{l_{11}s(\theta_{11}-\theta_{12})} & \frac{c(\theta_{12}-\theta_5)}{l_{11}s(\theta_{11}-\theta_{12})}b \\ \frac{-c(\theta_{22})}{l_{21}s(\theta_{21}-\theta_{22})} & \frac{-s(\theta_{22})}{l_{21}s(\theta_{21}-\theta_{22})} & \frac{c(\theta_{22}-\theta_5)}{l_{21}s(\theta_{21}-\theta_{22})}b \\ \frac{-c(\theta_{32})}{l_{31}s(\theta_{31}-\theta_{32})} & \frac{-s(\theta_{32})}{l_{31}s(\theta_{31}-\theta_{32})} & \frac{-c(\theta_{32}-\theta_5)}{l_{31}s(\theta_{31}-\theta_{32})}b \\ \frac{-c(\theta_{42})}{l_{41}s(\theta_{41}-\theta_{42})} & \frac{-s(\theta_{42})}{l_{41}s(\theta_{41}-\theta_{42})} & \frac{-c(\theta_{42}-\theta_5)}{l_{41}s(\theta_{41}-\theta_{42})}b \end{bmatrix} \tag{9}$$

The resultant forces and the resultant moment on the platform can be calculated as $\overline{F}_p = \overline{M}_I\ddot{\overline{u}}$, where $\ddot{\overline{u}} = [\ddot{x}_5, \ddot{y}_5, \ddot{\theta}_5]^T$ are the accelerations of the platform motion and $\overline{M}_I$ is the mass matrix

$$\overline{M}_I = \begin{bmatrix} m_5 + \sum_{i=1}^{4} m_{eq,i2} & 0 & 0 \\ 0 & m_5 + \sum_{i=1}^{4} m_{eq,i2} & 0 \\ 0 & 0 & I_5 + (\sum_{i=1}^{4} m_{eq,i2})b^2 \end{bmatrix} \tag{10}$$

with the equivalent masses $m_{eq,i2} = m_{i2}p_{i2}/l_{i2}$ of links $i2$ that are modeled in joints C_i as illustrated in Fig. 4b. From Eq. (4) $\overline{\tau}_I$ then is obtained as

$$(\overline{J}\dot{\overline{u}})^T\overline{\tau}_I \;=\; \dot{\overline{u}}^T\overline{M}_I\ddot{\overline{u}} \quad\Rightarrow\quad \overline{\tau}_I = \overline{J}^{T*}\overline{M}_I\ddot{\overline{u}} \tag{11}$$

with pseudo-inverse jacobian $\overline{J}^*$.

4.1.2. Actuator torques $\overline{\tau}_{II}$ for the motion of links $i1$

The actuator torques $\overline{\tau}_{II}$ for the motion of links $i1$ can be calculated with

$$\overline{\tau}_{II} \;=\; \overline{M}_{II}\ddot{\overline{q}} \tag{12}$$

For Peer Review

with $\ddot{\overline{q}} = [\ddot{\theta}_{11}, \ddot{\theta}_{21}, \ddot{\theta}_{31}, \ddot{\theta}_{41}]^T$ the vector of the angular accelerations of the driven links $i1$ and with mass matrix $\overline{M}_{II}$ written as

$$\overline{M}_{II} = \begin{bmatrix} I_{11} + m_{11}p_{11}^2 + I_{cm,1} + m_{cm,1}p_{cm,1}^2 + I_{act,1} + m_{eq,11}l_{11}^2 & 0 & 0 & 0 \\ 0 & I_{21} + m_{21}p_{21}^2 + I_{cm,2} + m_{cm,2}p_{cm,2}^2 + I_{act,2} + m_{eq,21}l_{21}^2 & 0 & 0 \\ 0 & 0 & I_{31} + m_{31}p_{31}^2 + I_{cm,3} + m_{cm,3}p_{cm,3}^2 + I_{act,3} + m_{eq,31}l_{31}^2 & 0 \\ 0 & 0 & 0 & I_{41} + m_{41}p_{41}^2 + I_{cm,4} + m_{cm,4}p_{cm,4}^2 + I_{act,4} + m_{eq,41}l_{41}^2 \end{bmatrix} \quad (13)$$

which includes the inertias $I_{i1} + m_{i1}p_{i1}^2$ of links $i1$ about joints A_i, the inertias $I_{cm,i}+m_{cm,i}p_{cm,i}^2$ of counter-masses i about joints A_i, the inertias $I_{act,i}$ of actuators i, and the inertias of the equivalent masses $m_{eq,i1} = m_{i2}(1 - p_{i2}/l_{i2})$ of links $i2$ that are modeled in joints B_i as shown in Fig. 4b. From Eq. (5) $\ddot{\overline{q}}$ can be derived as

$$\begin{aligned} \frac{d}{dt}(\overline{X}_n\dot{\overline{q}}) &= \frac{d}{dt}(\overline{Y}_n\dot{\overline{u}}) \\ \frac{d\overline{X}_n}{dt}\dot{\overline{q}} + \overline{X}_n\ddot{\overline{q}} &= \frac{d\overline{Y}_n}{dt}\dot{\overline{u}} + \overline{Y}_n\ddot{\overline{u}} \\ \ddot{\overline{q}} &= (\overline{X}_n)^{-1}(\frac{d\overline{Y}_n}{dt}\dot{\overline{u}} + \overline{Y}_n\ddot{\overline{u}} - \frac{d\overline{X}_n}{dt}\dot{\overline{q}}) \end{aligned} \quad (14)$$

with

$$\frac{d\overline{X}_n}{dt} = \begin{bmatrix} -l_{11}c(\theta_{11} - \theta_{12})(\dot{\theta}_{11} - \dot{\theta}_{12}) & 0 & 0 & 0 \\ 0 & -l_{21}c(\theta_{21} - \theta_{22})(\dot{\theta}_{21} - \dot{\theta}_{22}) & 0 & 0 \\ 0 & 0 & -l_{31}c(\theta_{31} - \theta_{32})(\dot{\theta}_{31} - \dot{\theta}_{32}) & 0 \\ 0 & 0 & 0 & -l_{41}c(\theta_{41} - \theta_{42})(\dot{\theta}_{41} - \dot{\theta}_{42}) \end{bmatrix} \quad (15)$$

$$\frac{d\overline{Y}_n}{dt} = \begin{bmatrix} -s(\theta_{12})\dot{\theta}_{12} & c(\theta_{12})\dot{\theta}_{12} & s(\theta_{12} - \theta_5)(\dot{\theta}_{12} - \dot{\theta}_5)b \\ -s(\theta_{22})\dot{\theta}_{22} & c(\theta_{22})\dot{\theta}_{22} & s(\theta_{22} - \theta_5)(\dot{\theta}_{22} - \dot{\theta}_5)b \\ -s(\theta_{32})\dot{\theta}_{32} & c(\theta_{32})\dot{\theta}_{32} & -s(\theta_{32} - \theta_5)(\dot{\theta}_{32} - \dot{\theta}_5)b \\ -s(\theta_{42})\dot{\theta}_{42} & c(\theta_{42})\dot{\theta}_{42} & -s(\theta_{42} - \theta_5)(\dot{\theta}_{42} - \dot{\theta}_5)b \end{bmatrix} \quad (16)$$

The angular velocities $\dot{\overline{q}}_2 = [\dot{\theta}_{12}, \dot{\theta}_{22}, \dot{\theta}_{32}, \dot{\theta}_{42}]^T$ of links $i2$ can be obtained from $l_{i2}\dot{\theta}_{i2} = -v_{t,i}^B + v_{t,i}^C$ with the velocity vectors $v_{t,i}^B$ and $v_{t,i}^C$ of joints B_i and C_i normal to line B_iC_i, respectively, as illustrated in Fig. 4a. In matrix notation this is written as

$$\overline{l}_2\dot{\overline{q}}_2 = -\overline{X}_t\dot{\overline{q}} + \overline{Y}_t\dot{\overline{u}} \qquad \Rightarrow \qquad \dot{\overline{q}}_2 = (\overline{l}_2)^{-1}(-\overline{X}_t\dot{\overline{q}} + \overline{Y}_t\dot{\overline{u}}) \quad (17)$$

For Peer Review

with

$$\overline{l}_2 = \begin{bmatrix} l_{12} & 0 & 0 & 0 \\ 0 & l_{22} & 0 & 0 \\ 0 & 0 & l_{32} & 0 \\ 0 & 0 & 0 & l_{42} \end{bmatrix} \overline{X}_t = \begin{bmatrix} l_{11}c(\theta_{11}-\theta_{12}) & 0 & 0 & 0 \\ 0 & l_{21}c(\theta_{21}-\theta_{22}) & 0 & 0 \\ 0 & 0 & l_{31}c(\theta_{31}-\theta_{32}) & 0 \\ 0 & 0 & 0 & l_{41}c(\theta_{41}-\theta_{42}) \end{bmatrix} \tag{18}$$

and

$$\overline{Y}_t = \begin{bmatrix} -s(\theta_{12}) & c(\theta_{12}) & s(\theta_{12}-\theta_5)b \\ -s(\theta_{22}) & c(\theta_{22}) & s(\theta_{22}-\theta_5)b \\ -s(\theta_{32}) & c(\theta_{32}) & -s(\theta_{32}-\theta_5)b \\ -s(\theta_{42}) & c(\theta_{42}) & -s(\theta_{42}-\theta_5)b \end{bmatrix} \tag{19}$$

The actuator torques $\overline{\tau}_{II}$ then are written as

$$\overline{\tau}_{II} = \overline{M}_{II}(\overline{X}_n)^{-1}(\frac{d\overline{Y}_n}{dt}\dot{\overline{u}} + \overline{Y}_n\ddot{\overline{u}} - \frac{d\overline{X}_n}{dt}\dot{\overline{q}}) \tag{20}$$

4.1.3. Actuator torques $\overline{\tau}_{III}$ for the rotational motion of links $i2$

The actuator torques for motion of the mass of links $i2$ is included in $\overline{\tau}_I$ and $\overline{\tau}_{II}$ with the equivalent masses in Fig. 4b. Then also a specific inertia of links $i2$ is included, which is the inertia of the equivalent model about its CoM calculated as $m_{eq,i1}p_{i2}^2 + m_{eq,i2}(l_{i2}-p_{i2})^2$. In general the real inertia of links $i2$ will not be equal to this value. This means that actuator torques $\overline{\tau}_{III}$ are required for the difference in the real inertia and the modeled inertia of links $i2$, which can be written in the mass matrix $\overline{M}_{III}$ as

$$\overline{M}_{III} = \begin{bmatrix} I_{12} - m_{eq,11}p_{12}^2 - m_{eq,12}(l_{12}-p_{12})^2 & 0 & 0 & 0 \\ 0 & I_{22} - m_{eq,21}p_{22}^2 - m_{eq,22}(l_{22}-p_{22})^2 & 0 & 0 \\ 0 & 0 & I_{32} - m_{eq,31}p_{32}^2 - m_{eq,32}(l_{32}-p_{32})^2 & 0 \\ 0 & 0 & 0 & I_{42} - m_{eq,41}p_{42}^2 - m_{eq,42}(l_{42}-p_{42})^2 \end{bmatrix} \tag{21}$$

The torques $\overline{\Gamma} = [\Gamma_1, \Gamma_2, \Gamma_3, \Gamma_4]^T$ that act on links $i2$ for rotational motion of this difference can be written as

$$\overline{\Gamma} = \overline{M}_{III}\ddot{\overline{q}}_2 \tag{22}$$

with angular accelerations $\ddot{\overline{q}}_2 = [\ddot{\theta}_{12}, \ddot{\theta}_{22}, \ddot{\theta}_{32}, \ddot{\theta}_{42}]^T$ of links $i2$ which can be derived from Eq. 17 as

$$\frac{d}{dt}(\overline{l}_2\dot{\overline{q}}_2) = \frac{d}{dt}(-\overline{X}_t\dot{\overline{q}} + \overline{Y}_t\dot{\overline{u}}) \Rightarrow \ddot{\overline{q}}_2 = (\overline{l}_2)^{-1}(-\frac{d\overline{X}_t}{dt}\dot{\overline{q}} - \overline{X}_t\ddot{\overline{q}} + \frac{d\overline{Y}_t}{dt}\dot{\overline{u}} + \overline{Y}_t\ddot{\overline{u}}) \tag{23}$$

For Peer Review

with

$$\frac{d\overline{X}_t}{dt} = \begin{bmatrix} -l_{11}s(\theta_{11}-\theta_{12})(\dot{\theta}_{11}-\dot{\theta}_{12}) & 0 & 0 & 0 \\ 0 & -l_{21}s(\theta_{21}-\theta_{22})(\dot{\theta}_{21}-\dot{\theta}_{22}) & 0 & 0 \\ 0 & 0 & -l_{31}s(\theta_{31}-\theta_{32})(\dot{\theta}_{31}-\dot{\theta}_{32}) & 0 \\ 0 & 0 & 0 & -l_{41}s(\theta_{41}-\theta_{42})(\dot{\theta}_{41}-\dot{\theta}_{42}) \end{bmatrix} \tag{24}$$

and

$$\frac{d\overline{Y}_t}{dt} = \begin{bmatrix} -c(\theta_{12})(\dot{\theta}_{12}) & -s(\theta_{12})(\dot{\theta}_{12}) & c(\theta_{12}-\theta_5)(\dot{\theta}_{12}-\dot{\theta}_5)b \\ -c(\theta_{22})(\dot{\theta}_{22}) & -s(\theta_{22})(\dot{\theta}_{22}) & c(\theta_{22}-\theta_5)(\dot{\theta}_{22}-\dot{\theta}_5)b \\ -c(\theta_{32})(\dot{\theta}_{32}) & -s(\theta_{32})(\dot{\theta}_{32}) & -c(\theta_{32}-\theta_5)(\dot{\theta}_{32}-\dot{\theta}_5)b \\ -c(\theta_{42})(\dot{\theta}_{42}) & -s(\theta_{42})(\dot{\theta}_{42}) & -c(\theta_{42}-\theta_5)(\dot{\theta}_{42}-\dot{\theta}_5)b \end{bmatrix} \tag{25}$$

The torque Γ_i on each link l_{i2} can be modeled with forces F_i in both B_i and C_i normal to line B_iC_i as illustrated in Fig. 4c. These forces are calculated with

$$\overline{F}_{III} = (\overline{l}_2)^{-1}\overline{\Gamma} \tag{26}$$

with $\overline{F}_{III} = [F_1, F_2, F_3, F_4]^T$. These forces determine the required actuator torques $\overline{\tau}_{III}$ and can be calculated in two parts. The forces F_i in B_i cause a direct torque onto the actuators which is written as

$$\overline{\tau}^a_{III} = -\overline{X}_t\overline{F}_{III} \tag{27}$$

The forces F_i in C_i act on the platform and therefore they can be distributed among the actuators with $\overline{J}^{T*}$ in a similar way as $\overline{\tau}_I$ was calculated, which results in

$$\overline{\tau}^b_{III} = \overline{J}^{T*}\overline{Y}^T_t\overline{F}_{III} \tag{28}$$

Altogether, the actuator torques $\overline{\tau}_{III}$ are calculated with

$$\overline{\tau}_{III} = \overline{\tau}^a_{III} + \overline{\tau}^b_{III} = (-\overline{X}_t + \overline{J}^{T*}\overline{Y}^T_t)\overline{F}_{III} \tag{29}$$

4.2. Simulation and validation of the inverse dynamic model

The DUAL-V manipulator was modeled with the multi-body simulation software package Spacar[1] and the simulation model is shown in Fig. 5. Since all mass and inertia data were modeled in the nodes, the shapes of the elements have no meaning.

[1] http://www.spacar.nl/

For Peer Review

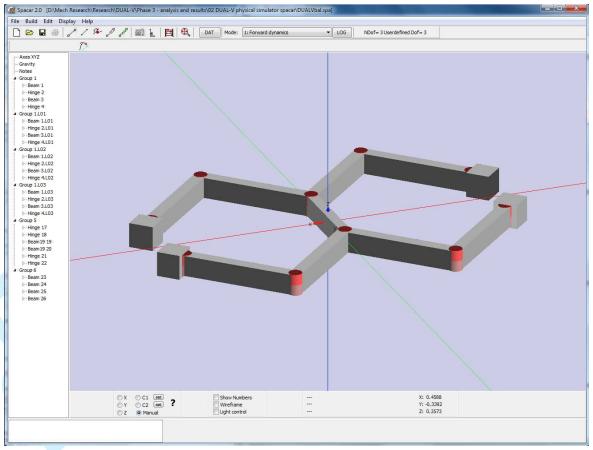

Figure 5: Spacar model of the balanced DUAL-V manipulator with mass and inertia modeled in the nodes.

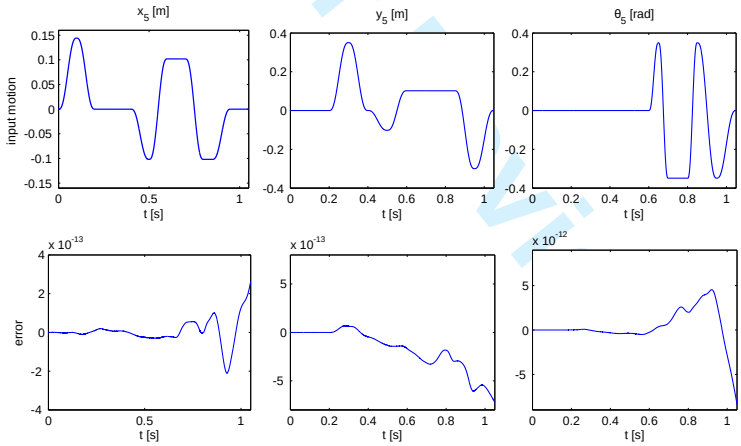

Figure 6: Validation of the inverse dynamic model for a motion throughout the workspace of the balanced manipulator. The error between the input platform motion and the **output platform motion** is in the order of the relative tolerance of the solver.

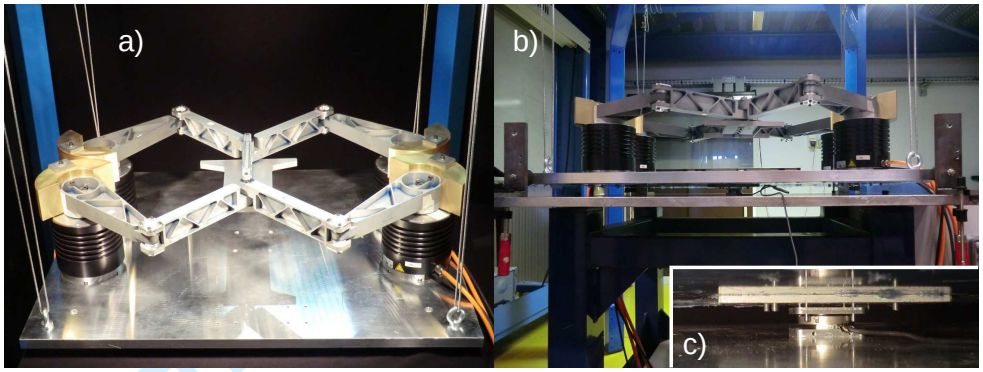

Figure 7: Experimental setup of the balanced prototype manipulator suspended by cables and mounted on a six-axes force/torque sensor for measurement of the in-plane shaking forces and shaking moment. a) overview; b) sideview; c) close-up of sensor mount.

Figure 6 shows the simulated motion for validation of the inverse dynamic model and the validation results. At each time step the actuator torques were calculated for a given platform motion and the dynamics were solved with solver ODE45 (Dormand-Prince), with maximal step size of $0.0001s$, and with a relative tolerance of $1e^{-12}m$. The results show the accuracy of the **output platform motion** with respect to the input platform motion, which is in the order of the relative tolerance of the solver. The platform motion consisted of accelerations up to $118m/s^2$ in x-direction, up to $202m/s^2$ in y-direction and up to $1612rad/s^2$ rotationally.

5. Experimental setup

The experimental setup of the prototype manipulator is shown in Fig.7. The manipulator of aluminium links and brass counter-masses was mounted on four *ETEL RTMB0140-100* direct drive actuators, which could deliver maximal torques of 127Nm. The actuators were mounted on an aluminum base plate of 1.0m by 0.8m with a thickness of 25mm. The unbalanced manipulator for comparison was the same manipulator but without the counter-masses and for evaluation of the sensitivity of the counter-masses on the shaking forces and the shaking moment, the tuning masses of lead were removed from the brass elements.

To measure the shaking forces and the shaking moment of the manipulator in the horizontal plane, an *ATI mini 45* six-axes force/torque sensor was positioned

For Peer Review

and centered between the base plate and the fixed frame (Fig. 7c). This sensor could measure a maximum of 500N shaking force in both x- and y- direction and 20Nm shaking moment with a measurement noise that was estimated to be about 3N and 0.02Nm. To unload the sensor from the gravity force, to align it horizontally, and to prevent damage during assembly, the base plate was suspended by four cables to float just above the sensor. Four pins fixed the sensor with respect to the base plate for in-plane motion while translation in vertical direction was not restricted.

The control of the manipulator was based on a PID-controller at a frequency of 10kHz. With the same frequency the actuator torques and the actuator orientations were recorded, while the measurement frequency of the force/torque sensor was 1kHz. With the information of the actuator encoders and the direct kinematic model the real manipulator motion was determined.

Since for high speed the PID-controller allowed significant trajectory deviations, for safety of not damaging the prototype, the experiments were limited to motion within a centered circular workspace with a diameter of 0.2m. From Fig. 8, which shows the condition number $\kappa = cond(\overline{J}_h)$ of the harmonized jacobian matrix $\overline{J}_h = \overline{J}[1, 0, 0; 0, 1, 0; 0, 0, 1/b]$ for three platform orientations, it can be observed that within this area the force transmission to the platform is optimal.

6. Experiments and experimental results

In this section the experiments are described and the results are presented. First various results of the shaking forces and the shaking moment are shown, followed by the results of the actuation torques and the results of the bearing forces. **The discussion of the results is in Section 7.**

For motion of the center of the platform along the orthogonal axes and without platform rotation, the unbalanced manipulator is expected to exhibit shaking forces and a zero shaking moment, of which the latter is because of the symmetric design. The balanced manipulator is expected to have zero shaking forces and a zero shaking moment.

Columns three and five in Fig. 9 show the measured shaking forces and shaking moment of the unbalanced and the balanced manipulator, respectively, for the motion shown in column one. This motion has maximal accelerations of $51m/s^2$ in both directions and $43rad/s^2$ rotationally, which therefore is not perfect balanced motion along the orthogonal axes. For validation, the shaking forces and

For Peer Review

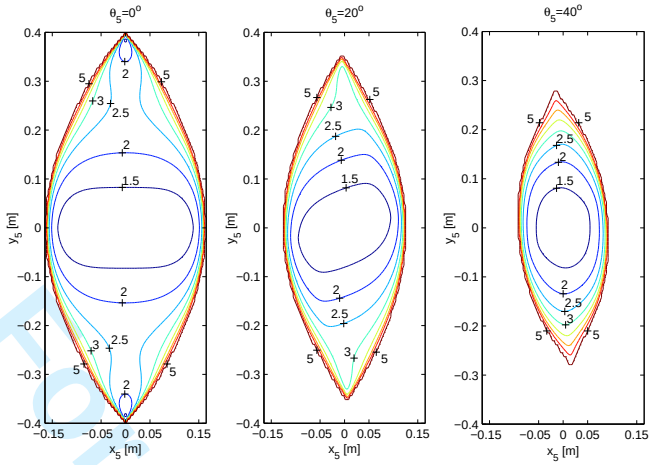

Figure 8: The condition number throughout the workspace for three platform orientations shows that the optimal dynamic performance is found in the center and along the y-axis.

the shaking moment of the unbalanced and the balanced manipulator from simulation of the measured motion are shown in column two and four, respectively.

For motion with non-rotated platform the unbalanced manipulator can be considered as a reduced mass m_{red} moving with the platform with which the expected shaking forces can be calculated. This reduced mass can be derived from the force-balance conditions in Eq. (1) or Eq. (2). For the unbalanced manipulator the product $m_{cm,i}p_{cm,i}$ is zero, which can also be interpreted as that factor $m_5 l_{i1}/2$ is increased with $m_{cm,i}p_{cm,i}$. Then the reduced mass representing the unbalanced manipulator can be obtained from $m_{red}l_{i1}/2 = m_{cm,i}p_{cm,i}$ as $m_{red} = 2m_{cm,i}p_{cm,i}/l_{i1} = 3.279kg$. The shaking forces of the unbalanced manipulator in Fig. 9 then are expected to be $51 \cdot 3.279 = 167N$.

A typical motion for pick and place tasks including referencing is motion along a triangular trajectory. Column one in Fig. 10 shows the measured motion of the manipulator when moved along a triangular trajectory with equal sides of $0.173m$ and with maximal accelerations of $66m/s^2$ along x, $63m/s^2$ along y, and $129rad/s^2$ rotationally. For the unbalanced and the balanced manipulator, the shaking forces and the shaking moment from simulation of the measured motion are shown in columns two and four, respectively, and the measured results

For Peer Review

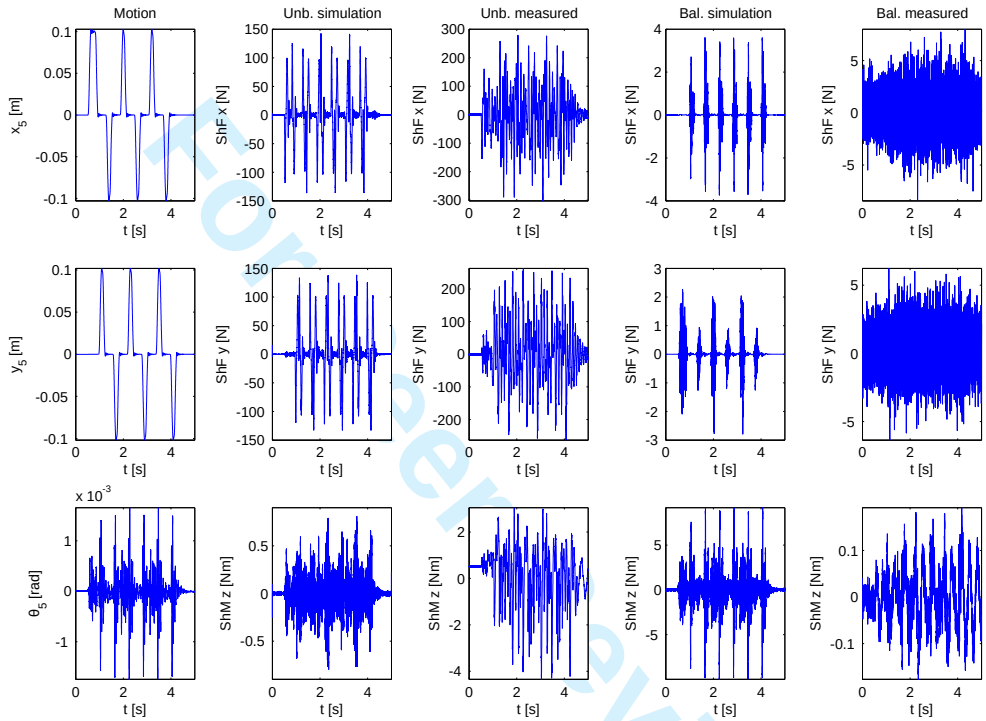

Figure 9: Results from simulation and experiments of the unbalanced and the balanced manipulator for the measured motion in column one, which is motion along the orthogonal axes with maximal accelerations of $51m/s^2$ and $43rad/s^2$ rotationally. It shows that the measured shaking forces of the balanced manipulator are 97% and 98% lower in x- and y-direction, respectively, and the measured shaking moment is 96% lower as compared to the unbalanced manipulator.

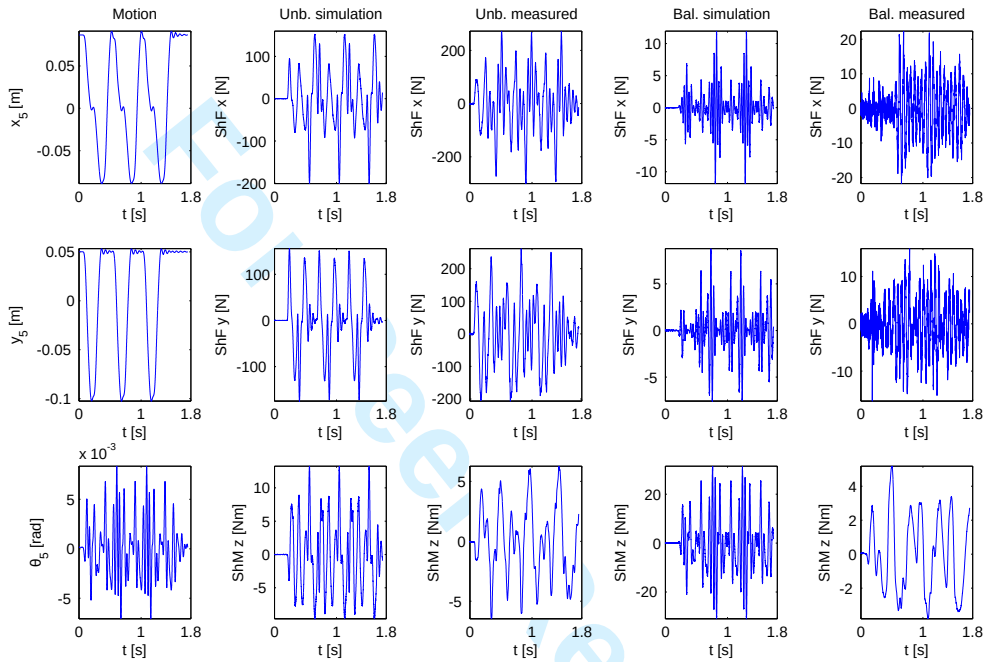

Figure 10: For the measured motion with maximal accelerations of $66m/s^2$ along x, $63m/s^2$ along y, and $129rad/s^2$ rotationally along a triangular trajectory with equal sides of $0.173m$ in column one, columns two and four show the simulation results and columns three and five show the experimental results for the unbalanced and the balanced manipulator, respectively. For the balanced manipulator the measured shaking forces are 93% and 94% lower in x- and y-direction, respectively, and the measured shaking moment is 16% lower as compared to the unbalanced manipulator.

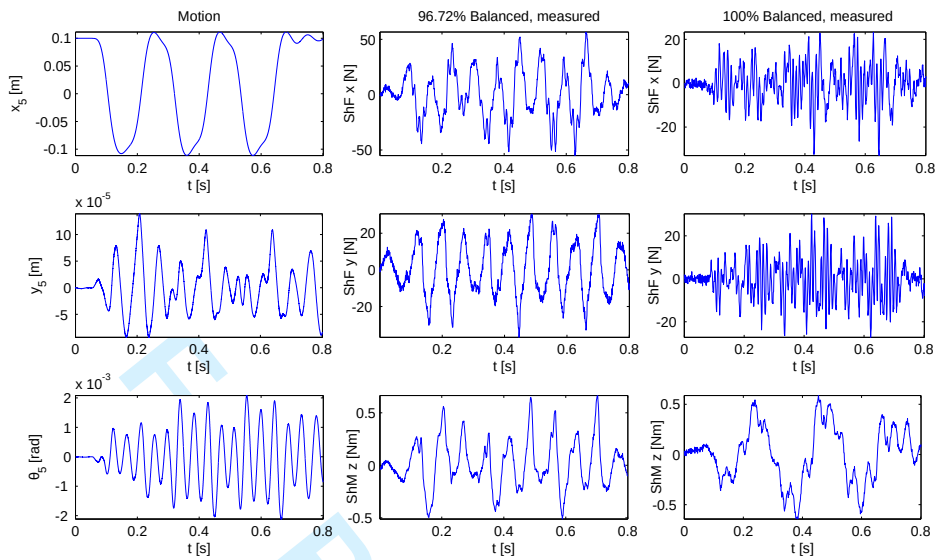

Figure 11: Experimental results of the 96.72% balanced manipulator and of the fully balanced manipulator for the motion in column one with maximal accelerations of $186m/s^2$ along x, $3m/s^2$ along y, and $50rad/s^2$ rotationally. The maximal shaking forces of the 96.72% balanced manipulator are increased with 73% along x and 23% along y, while maximal shaking moment is reduced with 13%.

are shown in columns three and five, respectively. When the platform rotation would be zero, the unbalanced manipulator is expected to have shaking forces of $66 \cdot 3.279 = 216N$ along x and $63 \cdot 3.279 = 207N$ along y and the balanced manipulator is expected to exhibit only a shaking moment, while shaking forces are zero.

To evaluate the sensitivity of the balance masses, the tuning-masses were removed from each counter-mass for which each product $m_{cm,i}p_{cm,i}$ is 96.72% of the value for perfect balance, or has a 3.28% balance inaccuracy. Fig. 11 shows the experimental results of this 96.72% balanced manipulator and of the fully balanced manipulator for the motion in column one which has maximal accelerations of $186m/s^2$ along x, $3m/s^2$ along y, and $50rad/s^2$ rotationally.

The results in Fig. 11 also represent the influence of payload on the platform. An equal 3.28% balance inaccuracy is also obtained by placing $0.107kg$ in the center of the platform, instead of leaving the tuning masses out. This is calculated similarly as for the reduced mass of the unbalanced manipulator as

For Peer Review

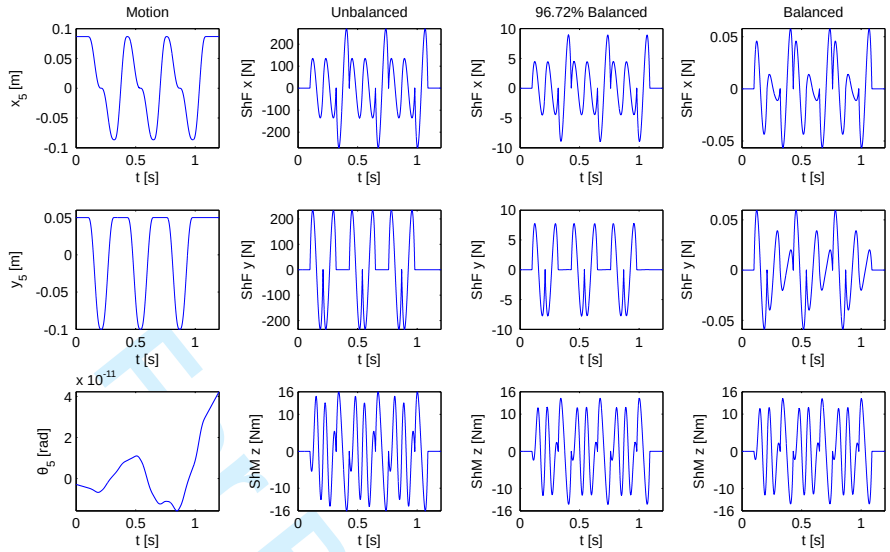

Figure 12: Theoretical simulation results of the inverse dynamic model of the unbalanced, the 96.72% balanced, and the fully balanced manipulator for the motion in column one with maximal accelerations of $82.6m/s^2$ and $71.6m/s^2$ in x- and y-direction, respectively. 96.72% balance represents $0.107kg$ of unbalanced mass on the platform for which the shaking forces increase considerably. The shaking moment of the balanced manipulator is 12% lower as compared to the unbalanced manipulator.

$2m_{tun,i}p_{tun,i}/l_{i1} = 2 \cdot 0.188 \cdot 0.080/0.280 = 0.107kg$. By moving this mass with $186m/s^2$ along x, a shaking force of $186 \cdot 0.107 = 20N$ is expected.

For comparison, Fig. 12 shows the theoretical simulation results of the inverse dynamic model for the smooth motion along the triangular trajectory of column one with maximal accelerations of $82.6m/s^2$ and $71.6m/s^2$ in x- and y-direction, respectively. The shaking forces and the shaking moment of the unbalanced manipulator, of the 96.72% balanced manipulator, and of the fully balanced manipulator are shown in columns two, three, and four, respectively. Here the shaking forces of the unbalanced manipulator are expected to be $82.6 \cdot 3.279 = 271N$ and $71.6 \cdot 3.279 = 235N$ in x- and y- direction, respectively, while for the 96.72% balanced manipulator they are expected to be $82.6 \cdot 0.107 = 8.9N$ and $71.6 \cdot 0.107 = 7.7N$ in x- and y-direction, respectively.

Since the balance masses add inertia to the manipulator, the balanced manipu-

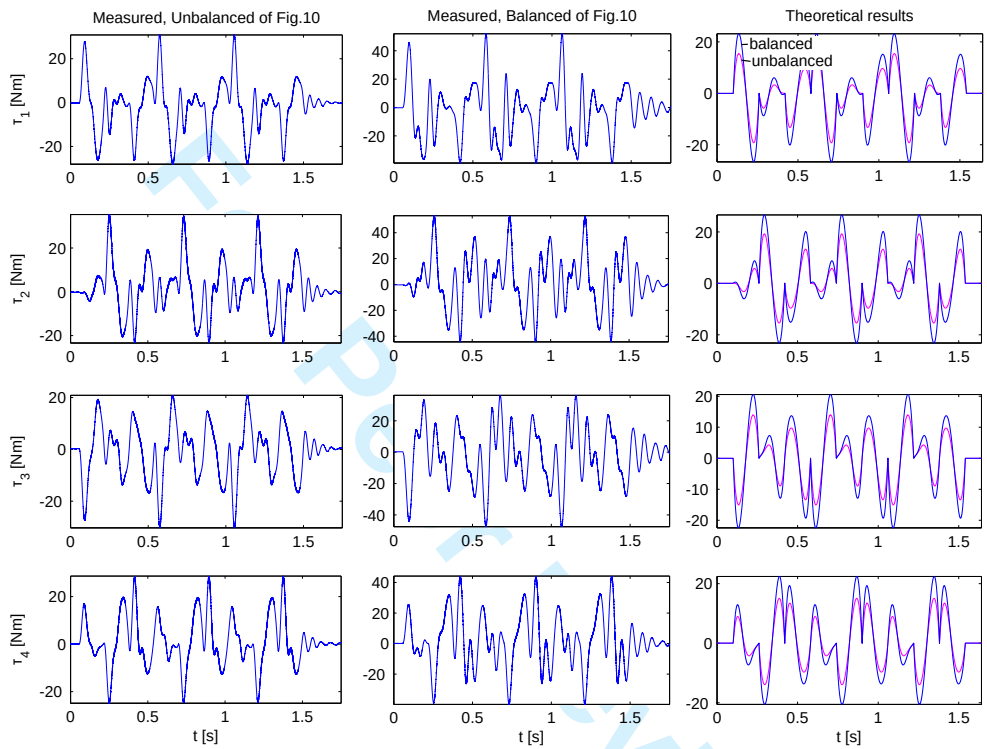

Figure 13: For the motion in Fig. 10 the measured actuator torques of the unbalanced and the balanced manipulator are shown in columns 1 and 2, respectively. Column 3 shows the actuator torques of both manipulators from the inverse dynamic model for equal input motion. The smaller curves represent the unbalanced manipulator. From experiments the actuator torques of the balanced manipulator are about 1.6 times higher while theoretically they are about 1.4 times higher than the actuator torques of the unbalanced manipulator.

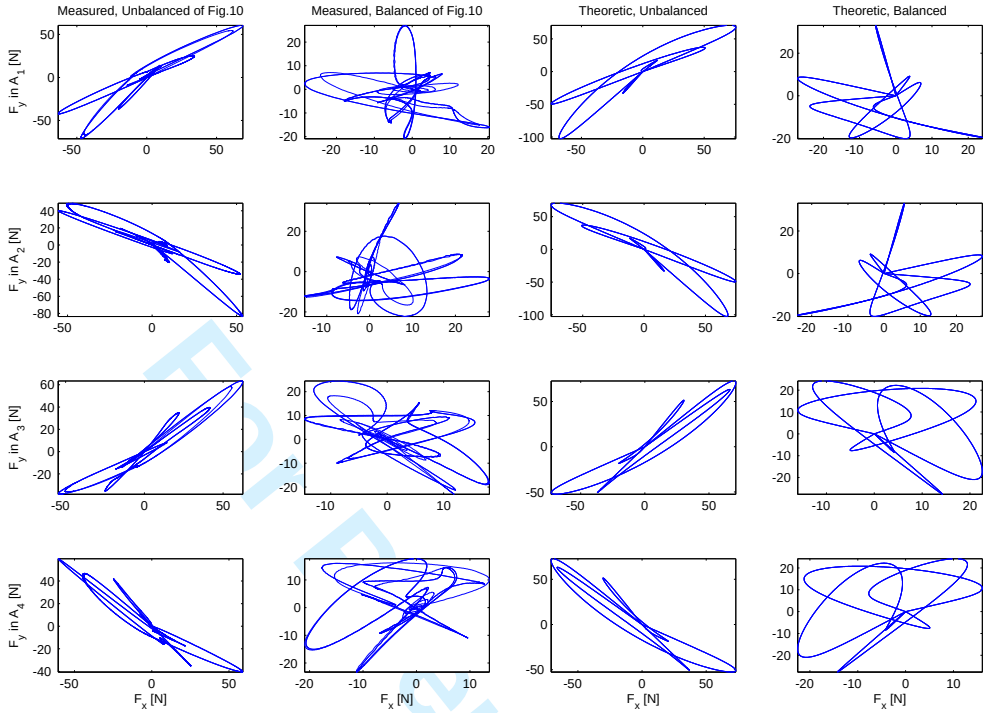

Figure 14: For the motion in Fig. 10, the bearing forces from simulation of the measured motion of the unbalanced and the balanced manipulator are shown in columns one and two, respectively. Columns three and four show the results from simulation of smooth motion along the triangular trajectory with equal maximal accelerations. It is found that the maximal bearing forces of the balanced manipulator are 73% lower in joints A_1 and A_2 and are 69% lower in joints A_3 and A_4 as compared to the unbalanced manipulator.

lator is expected to require higher actuator torques. For the motion in Fig. 10, the measured actuator torques of the unbalanced manipulator and the balanced manipulator are shown in columns one and two in Fig. 13, respectively. Column three shows the actuator torques of both manipulators calculated from the inverse dynamic model for equal input motion. The smaller curves represent the unbalanced manipulator.

The improved mass distribution due to the counter-masses is expected to have an advantageous influence on the bearing forces of the balanced manipulator. For simulations of the measured motion in Fig. 10, columns one and two in Fig. 14 show the bearing forces of the unbalanced and the balanced manipulator, respec-

For Peer Review

tively. For validation, columns three and four show the bearing forces from the simulations for smooth motion along the triangular trajectory with equal maximal accelerations.

7. Discussion

In this section the experimental results are discussed. First the shaking forces and the shaking moment are considered and subsequently the sensitivity to unbalance, the actuator torques, and the bearing forces are treated. Also the design approaches and evaluation method are discussed.

7.1. Shaking forces and shaking moments

The measurements in Fig. 9 show a significant reduction of the shaking forces of the balanced manipulator. While for the unbalanced manipulator the maximal measured shaking forces are 302N along x and 263N along y, the balanced manipulator has maximal shaking forces of 8.4N along x and 6.4N along y, being close to the noise level of the sensor. This means a reduction of 97% and 98% of shaking forces along x and y, respectively. The shaking forces of the balanced manipulator are nonzero mainly due to the rotational motion of the platform.

From simulation of the measured motion, the maximal shaking forces of the unbalanced manipulator are about 142N along x and 138N along y (column three) while for the balanced manipulator they are about 3.7N along x and 2.8N along y (column four). Also for these values the reduction of shaking forces is 97% and 98% along x and y, respectively, however the values differ significantly from the measured maximal values. Also both values of the unbalanced manipulator differ from the expected 167N shaking forces. Most likely this is caused by the calculations of the derivative (velocity) and the second derivative (acceleration) of the measured motion, which are needed for the inverse dynamic model. Since the derivatives of the measured position information result in unrealistically high values, the values were filtered with a first order low pass filter. However the simulation results show that this is not sufficient. In addition, the mentioned maximal accelerations were obtained from these derivatives, which explains why the expected shaking forces are closer to the results of the simulation of the measured motion.

The measured shaking moment of the unbalanced manipulator has a maximal value of 4.3Nm, while for the balanced manipulator it is at most 0.19Nm, which is 96% lower. It is likely that the measurements of the unbalanced manipulator

For Peer Review

are affected significantly by frame vibrations. In the experimental setup the relatively large inertia of the manipulator with the base plate in combination with the stiffness of the force/torque sensor caused the base plate to rotate in the lowest eigenmode with measured eigenfrequency of about 3.4Hz. This may have caused interference of the relatively high shaking forces with the measured shaking moment.

The simulation results of the shaking moment (column two and four) are dramatically affected by the mentioned differentiation problem. Although the values of the unbalanced manipulator could be realistic, the values of the balanced manipulator are, with a maximal value of 10Nm, significantly higher as compared to the measured values. The shaking moment is obtained from the simulation as the sum of the actuator torques together with the moments created by the individual reaction forces in A_i with respect to the center. Due to the differentiation problem, all individual reaction forces are affected for which the resulting shaking moments become useless.

For motion along the triangular trajectory, Fig. 10 shows that the measured shaking forces of the balanced manipulator have maximal values of 22N along x and 16N along y, which are nonzero because of rotational motion of the platform. Compared with the unbalanced manipulator showing maximal measured shaking forces of 300N along x and 262N along y, the balanced manipulator has 93% and 94% reduced shaking forces, respectively. The maximal measured shaking moment of the unbalanced manipulator is 6.5Nm while of the balanced manipulator it is 5.2Nm, which is 16% lower.

From the simulations in columns two and four, the unbalanced manipulator has maximal shaking forces of 200N along x and 175N along y, while for the balanced manipulator the maximal shaking forces are 12N along x and 8.8N along y. This results in 94% and 95% reduced shaking forces along x and y, respectively, for which they differ 1% from the results from the measurements. Regarding the simulated results, the same remarks apply as for Fig. 9, for which the simulated shaking moments cannot be interpreted.

From the theoretical simulation of motion along the triangular trajectory in Fig. 12, the unbalanced manipulator has maximal shaking forces of 271N along x and 235N along y, as expected, while the balanced manipulator has minimal shaking forces. The maximal shaking moment of the unbalanced manipulator is 16.1Nm while the maximal shaking moment of the balanced manipulator is 14.1Nm which is 12% lower. This is less than the measured difference in maximal shaking moment of 16% in Fig. 10.

For Peer Review

7.2. Sensitivity

The sensitivity of the dynamic balance was investigated for a balance inaccuracy of 3.28%, representing the effect of inaccurate counter-masses that are $0.188kg$ too lightweight or of a payload of $0.107kg$ on the platform. The results in Fig. 11 show that for 3.28% balance inaccuracy, the shaking forces increase from maximal values of 33N along x and 30N along y (column three) to maximal values of 57N along x and 37N along y (column two). This means an increase of shaking forces of 73% along x and 23% along y. The difference in shaking force along x is $57N - 33N = 24N$ and close to the expected 20N shaking force for the 3.28% balance inaccuracy. The maximal shaking moment shows to be reduced from 0.64Nm (column three) to 0.56Nm (column two) which is a reduction of 13%.

The theoretical simulation of motion along the triangular trajectory in Fig. 12 shows that the 96.72% balanced manipulator has maximal shaking forces of 8.9N along x and 7.7N along y, as expected from the calculations from the force-balance conditions. This means that the expected shaking forces of the manipulator for motion without rotation of the platform can be described as

$$\begin{bmatrix} ShF_x \\ ShF_y \end{bmatrix} = \frac{2(m_{cm,i}p_{cm,i})^{dif}}{l_{i1}} \begin{bmatrix} \ddot{x}_5 \\ \ddot{y}_5 \end{bmatrix} = m_{payload} \begin{bmatrix} \ddot{x}_5 \\ \ddot{y}_5 \end{bmatrix} \tag{30}$$

showing a linear relation between the shaking forces ShF_x and ShF_y and the balance inaccuracy or difference from perfect balance $(m_{cm,i}p_{cm,i})^{dif}$ and the payload $m_{payload}$ on the platform. The maximal shaking moment of the 96.72% balanced manipulator in Fig. 12 is 14.2Nm, which is, contrary to the measured results, about 1% higher than of the fully balanced manipulator.

Due to the PID-controller that allowed the manipulator to move not perfectly along the desired trajectories, from the results in Figs. 9, 10, and 11 also the sensitivity to motion inaccuracy is shown. For motion not perfectly along the orthogonal axes, Fig. 9 shows that shaking moments exist which however remain small as compared to the motion in Fig. 10. Also the sensitivity to rotation of the platform is shown. Small rotations of the platform can already contribute significantly to the shaking forces since measured shaking forces of the balanced manipulator in Figs. 9, 10, and 11 are not zero as expected.

Altogether it can be concluded that small inaccuracies of the counter-masses, of unbalanced payload on the platform, and of platform rotations can already lead to considerable vibrations for high-speed manipulations al-

For Peer Review

though they remain significantly low as compared to the unbalanced manipulator. Therefore a high accuracy of the design, of the production, and of the control of a balanced manipulator is important for optimal dynamic balance.

7.3. Actuator torques

The measured actuator torques in Fig. 13 show that the torques required to move the balanced manipulator are higher than the torques of the unbalanced manipulator. The maximal values of the torques τ_1, τ_2, τ_3, and τ_4 of the unbalanced manipulator are 31Nm, 35Nm, 30Nm, and 29Nm, respectively, and of the balanced manipulator they are 52Nm, 53Nm, 47Nm, and 44Nm, respectively. This means that for the balanced manipulator they are 1.68, 1.51, 1.57, and 1.52 times the torques of the unbalanced manipulator, respectively, which is on average 1.6 times higher.

From the theoretical results in column 3 in Fig. 13, the maximal torques τ_1 and τ_2 are both 1.42 times higher being 27Nm and maximal torques τ_3 and τ_4 are both 1.47 times higher being 22Nm, which is on average 1.4 times higher for the balanced manipulator. The actuator torques from the theoretical results are lower than the measured torques which may be caused by the high torques that the PID-controller calculates to correct the output motion and by friction which was not included in the calculations with the inverse dynamic model.

7.4. Bearing forces

The bearing forces shown in column one and two in Fig. 14 were derived from the simulation of the real motion in Fig. 10. Since the values of the shaking forces from these simulations have been considered to be inaccurate due to the differentiation problem, also the values of the individual bearing forces are inaccurate. However the results from the simulation in Figs. 9 and 10 have shown to be suitable for comparing the unbalanced and the balanced manipulator.

For simulation of precise motion along the triangular trajectory with equal accelerations, columns three and four of Fig. 14 show the bearing forces of which the shapes and size are comparable with columns one and two. From both simulations it is found that the maximal bearing forces in A_1 and A_2 are 73% lower and in A_3 and A_4 are 69% lower for the balanced manipulator. The maximal forces were calculated as $max(\sqrt{F_x^2 + F_y^2})$ in each bearing. The lower bearing forces imply that the balanced manipulator has increased stiffness characteristics.

For Peer Review

7.5. *Design approaches and evaluation method*

The approaches to the design of balanced manipulators have resulted in a new manipulator which was shown to be both feasible for high speed tasks and to have low vibration of the base. **The aim was to have a perfectly dynamically balanced manipulator along the orthogonal axes. Since all motion of the manipulator remains in the vicinity of perfect balance, the manipulator showed to have significant balance performance throughout the workspace.**

The design approaches can be applied for the synthesis of other planar and spatial dynamically balanced multi-DoF parallel manipulators. For planar manipulators the linear momentum equations can be investigated to find the optimal kinematic and dynamic parameters of an initial configuration. This approach may be challenging for spatial manipulators since their linear momentum equations can be complex. Composing spatial manipulators of known balanced architectures then may be more advantageous. To obtain spatial mechanisms with desired mobility together with optimal similar opposite motions of the masses and inertias, for which advantageous balance solutions are found, still is a challenge of future research.

The evaluation method of considering the measured motion of the manipulator and using this motion as input for the simulations showed to be partly successful. Since only position data of the manipulator motion were recorded, these data had to be differentiated twice to obtain the velocity data and the acceleration data at each time step. Because of this, the obtained values for the shaking forces and shaking moment were not equal to the measured values. However, the resulting shaking forces from simulations showed to be applicable for the relative comparison of the balanced and the unbalanced manipulator. This was not true for the shaking moments. Therefore, for a better application of this evaluation method, it is required to have accurate velocity and acceleration data, for example by measuring as well the position, the velocity, and the acceleration of the manipulator motion during experiments with additional sensors.

8. Conclusion

The design of a dynamically balanced redundant planar 4-RRR parallel manipulator was presented together with the design approaches of adapting a given kinematic architecture and of composing it from known balanced architectures. A prototype manipulator in an experimental setup was presented for evaluation and comparison of the balanced manipulator with the unbalanced manipulator. A method was proposed for a fair evaluation and comparison in which the measured

For Peer Review

motion from the experiments was used as input for the simulation. For precise simulation of the manipulator motion, the inverse dynamic model of the manipulator was derived and validated.

The prototype manipulator successfully performed high speed motion with low base vibration. Experiments showed that the balanced manipulator has about 97% lower shaking forces and a 96% lower shaking moment for motion along the orthogonal axes. For motion throughout the workspace, the balanced manipulator showed about 93% lower shaking forces and 16% lower shaking moment. Since the PID-controller allowed small rotational motion of the platform, causing shaking forces, it is expected that these values will reduce further when the control of the rotation of the platform is improved.

A relatively small balance inaccuracy of 3.28%, representing too light countermasses or an unbalanced payload on the platform, showed to increase the shaking forces considerably, while they still remain significantly low as compared to the unbalanced manipulator. **For a manipulator with optimal dynamic balance, accurate design and production therefore are important.** The actuator torques of the balanced manipulator were shown to be about 1.6 times higher than for the unbalanced manipulator and the bearing forces of the balanced manipulator were shown to be about 71% lower than for the unbalanced manipulator.

It was found that shaking forces and shaking moments obtained from precise simulation of the measured manipulator motion with the inverse dynamic model are affected by the differentiation of the measured position data to obtain velocities and accelerations. The obtained values showed to be useful for the relative comparison of the shaking forces of the balanced and the unbalanced manipulator, but their values were not equal to the measured values. Hence the simulated results of the shaking moments showed to be useless.

Supplementary content

A video of the prototype manipulator is available on the IJRR website (www.ijrr.org), showing the unbalanced motion and the balanced motion of Fig. 9 and the balanced motion of Fig. 11.

References

Agrawal, S. K., Gardner, G., Pledgie, S., 2001. Design and fabrication of an active gravity balanced planar mechanism using auxiliary parallelograms. Mechanical Design 123, 525–528.

For Peer Review

Arakelian, V. G., Smith, M. R., 2005a. Shaking force and shaking moment balancing of mechanisms: A historical review with new examples. Mechanical Design 127, 334–339.

Arakelian, V. H., Smith, M. R., 2005b. Erratum: Shaking force and shaking moment balancing of mechanisms: A historical review with new examples. Mechanical Design 127, 1035.

Briot, S., Arakelian, V. H., Guégan, S., 2009. PAMINSA: A new family of partially decoupled parallel manipulators. Mechanism and Machine Theory 44, 425–444.

Chung, W.-K., Cho, H. S., May 1988. On the dynamic characteristics of a balanced PUMA-760 robot. Industrial Electronics 35 (2), 222–230.

Corbel, D., Gouttefarde, M., Company, O., Pierrot, F., May 2010. Towards 100G with PKM. is actuation redundancy a good solution for pick-and-place? Proc. of the IEEE International Conference on Robotics and Automation, Anchorage, USA, 4675–4682.

Demeulenaere, B., Berkof, R. S., August 2008. Improving machine drive dynamics: A structured design approach toward balancing. Mechanical Design 130 (082302).

Fischer, O., 1906. Theoretische grundlagen für eine Mechanik der lebenden Körper. Teubner, Leipzig.

Foucault, S., Gosselin, C. M., 2004. Synthesis, design, and prototyping of a planar three degree-of-freedom reactionless parallel mechanism. Mechanical Design 126, 992–999.

Jean, M., Gosselin, C. M., 1996. Static balancing of planar parallel manipulators. Proc. of Int. Conference on Robotics and Automation, 3732–3737.

Lim, T. G., Cho, H. S., Chung, W. K., 1989. A parameter identification method for robot dynamic models using a balancing mechanism. Robotica 7, 327–337.

Lim, T. G., Cho, H. S., Chung, W. K., 1990. Payload capacity of balanced robotic manipulators. Robotica 8, 117–123.

Ricard, R., Gosselin, C. M., 2000. On the development of reactionless parallel manipulators. Proc. of ASME-DETC (DETC2000/MECH-14098).

For Peer Review

Van der Wijk, V., Demeulenaere, B., Gosselin, C., Herder, J. L., 2012. Comparative analysis for low-mass and low-inertia dynamic balancing of mechanisms. Mechanisms and Robotics 4 (3, 031008).

Van der Wijk, V., Herder, J. L., 2008. Dynamic balancing of mechanisms by using an actively driven counter-rotary counter-mass for low mass and low inertia. Proc. of the Second Int. Workshop on Fundamental Issues and Future Research Directions for Parallel Mechanisms and Manipulators, Montpellier, 241–251.

Van der Wijk, V., Herder, J. L., 2009. Guidelines for low mass and low inertia dynamic balancing of mechanisms and robotics. In: Kröger and Wahl, Advances in Robotics Research, Proc. of the German Workshop on Robotics, 21–30Springer, ISBN 978-3-642-01212-9.

Van der Wijk, V., Herder, J. L., 2012a. Inherently balanced 4R four-bar based linkages. In: Lenarčič, J. and Husty, M. (Eds.), Latest Advances in Robot Kinematics, Proc. of the IFToMM 13th Int. Symposium on Advances in Robot Kinematics, 309–316Springer, ISBN 978-94-007-4619-0.

Van der Wijk, V., Herder, J. L., 2012b. Synthesis method for linkages with center of mass at invariant link point - pantograph based mechanisms. Mechanism and Machine Theory 48, 15–28.

Van der Wijk, V., Herder, J. L., Demeulenaere, B., 2009. Comparison of various dynamic balancing principles regarding additional mass and additional inertia. Mechanisms and Robotics 1 (4), 04 1006.

Van der Wijk, V., Krut, S., Pierrot, F., Herder, J. L., 2011. Generic method for deriving the general shaking force balance conditions of parallel manipulators with application to a redundant planar 4-RRR parallel manipulator. Proceedings of the 13th IFToMM World Congress on Mechanism and Machine Science, Guanajuato, Mexico (A12-523).

For Peer Review